INORGANIC CHEMISTRY FRONTIERS

RESEARCH ARTICLE

View Article Online
View Journal

Cite this: DOI: 10.1039/d5qi02109j

At the intersection of X- and Z-type ligands: an inverted ligand field in carbene-supported borylnickel complexes

YuXiang Wei,[a] Elizabeth McKenzie,[a] Vignesh Pattathil,[a] Junyi Wang,[b] Robert K. Szilagyi[a] and Conor Pranckevicius *[a]

Received 15th October 2025,
Accepted 28th November 2025

DOI: 10.1039/d5qi02109j

rsc.li/frontiers-inorganic

The first examples of NHC-supported borylnickel complexes have been accessed *via* the reaction of a phosphine-tethered carbene-bromoborane adduct and a Ni(0) source. DFT calculations and Ni K- and L-edge XANES data indicate that there is significant Ni(0) character in the resulting complexes, and that the boryl ligand in this case is best regarded as a Z-type acceptor ligand. Reactivity studies of this novel complex have found an unprecedented insertion product with an aryl isocyanide forming an 8-membered metallocycle, and a Ni abnormal-carbene complex has also been accessed from an analogous reaction with a chloroborane precursor.

Introduction

Nickel and boron form energetically high-lying and reactive bonds that have been shown to participate in the cooperative activation of inert substrates.[1] Complexes featuring Ni–B bonds have found use in a growing number of transformations including catalytic C–X borylation reactions (X = H, F, Cl),[2–8] olefin hydrogenation,[9–12] ethylene oligomerization,[13,14] and CO_2 cleavage.[15] Nickel–boron bonds are commonly classified according to whether the boron atom accepts electron density from Ni as a Z-type acceptor ligand,[16,17] or whether boron possesses a lone pair that donates into nickel within a neutral (borylene; L-type), or anionic (boryl; X-type) formally B(I) ligand.[18–24]

While nickel borylenes are rare species that have only been isolated in a few instances,[25–27] borylnickel complexes are known to be important intermediates in numerous catalytic transformations, and a handful of these complexes have been isolated and fully characterized.[10,11,14,28–33] Common ligands include pinacolboryl, catecholboryl, and 1,3,2-diazaborol-2-yls, where the electron-rich boron centre is further stabilized by the presence of two neighboring electronegative atoms (Fig. 1A and B). When complexed with boryl ligands, Ni is found in the formal +II oxidation state and adopts a nearly square planar geometry in all known examples.

Conversely, trivalent tricoordinate boranes may also accept electron density from electron-rich nickel(0) centres as Z-type ligands, where the nickel is formally assigned a lone pair of electrons.[34–37] In nearly all cases, Lewis-acidic tricoordinate borane ligands are held in the coordination sphere of nickel *via* chelating L-type donor ligands (Fig. 1C). Notably, the first examples of complexes featuring monodentate κ^1-Ni→BR_3 interactions were recently isolated by Hoshimoto and co-

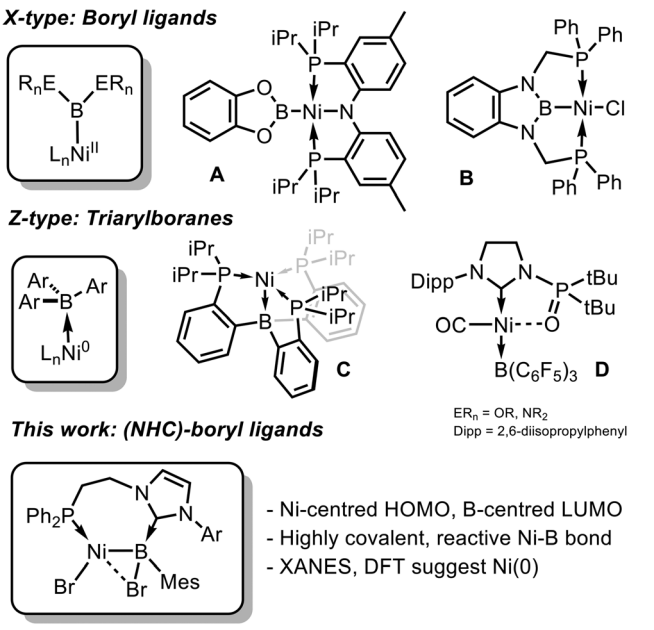

Fig. 1 Electron-precise bonding modes of Ni and B.

[a]Department of Chemistry, Charles E. Fipke Centre for Innovative Research, University of British Columbia, Okanagan Campus, 3247 University Way, Kelowna, BC, Canada. E-mail: conor.pranckevicius@ubc.ca
[b]Department of Chemistry and Biochemistry, Baylor University, 1 Bear Place, Waco, Texas, USA

workers and feature an unusual square planar geometry, where secondary binding interactions anchor the borane within the coordination sphere of nickel (Fig. 1D).[38] Bourissou and coworkers have also prepared Au(I) and Pt(0) complexes supported by L_2Z-type acceptor ligands that similarly feature atypical d^{10} square planar geometries.[39,40]

These X/Z ligand descriptions stem from the formal assignment of a lone pair of electrons to either the boron or nickel centre, and are often intuitively guided by the stability of the boron ligand in the absence of transition metal binding – indeed, Z-type borane ligands are readily isolated in the absence of metal coordination. Additionally, the isolation of a stable Group I diaminoboryl by Nozaki and coworkers highlights the thermodynamic stability of two-coordinate boryl anions flanked by electronegative atoms.[41] While there is significant covalency inherent in nickel–boron bonding,[42] it is the coordination number and electronic environment at boron that has been used to favor one ligand description over another in these complexes.

N-Heterocyclic carbenes (NHCs) have a longstanding history of stabilizing both electron-rich and electron-poor main group centres *via* their strong σ-donor and tuneable π-acceptor properties.[43–45] In the case of boron, this has resulted in stabilization and isolation of multiple formal "oxidation states" of [(NHC)BR_2] moieties, from borenium, to boryl radical, to boryl anion.[46–57] While NHC-boryl ligands have been previously accessed in the form of [Cp*Fe$(CO)_2$(BX_2(NHC))] complexes (X = H, Cl),[58,59] and a recent report by Lyu of a [Cu(BH_2(NHC))] tetramer,[60] we noted that some [(NHC)BR_2]$^+$ ions are reported to be *less* electrophilic than electron poor triarylboranes such as $B(C_6F_5)_3$,[50] suggesting they should act as Z-type acceptor ligands with the more electronegative metals such as nickel and copper. It has also recently been reported that nickel–boryl and borane complexes display distinctly different electronic tuning effects in hydrogenation catalysis,[12] and that understanding the boundaries of these ligand types is key to the design of efficient catalysts. To probe the limits of Z- and X-type ligand descriptions within nickel-boron complexes, we became interested in constructing such a ligand, where both Z-type and X-type ligand "oxidation states" could be chemically reasonable. We further envisioned a system tethered to the metal centre *via* a flexible linker to facilitate, but not to enforce coordination of the boron moiety. Herein, we report the first examples of [(NHC)BR_2] complexes of nickel and characterize the bonding and reactivity of these highly covalent nickel–boron species.

Results and discussion

To construct an appropriate ligand precursor, $MesBBr_2$ was added to solutions of the phosphino–carbenes $\mathbf{1}^{\mathbf{Mes}}$ and $\mathbf{1}^{\mathbf{Dipp}}$, selectively forming the corresponding boronium salts $\mathbf{2}^{\mathbf{Mes}}$ and $\mathbf{2}^{\mathbf{Dipp}}$ (Scheme 1). In the case of $\mathbf{1}^{\mathbf{Mes}}$ the carbene was generated *in situ* due to its instability in free form, whereas for $\mathbf{1}^{\mathbf{Dipp}}$ it was isolated. Phosphine coordination to the borane was confirmed through a single crystal X-ray diffraction study of $\mathbf{2}^{\mathbf{Dipp}}$ (Fig. S24 in the SI) and its C_1 symmetry was evidenced by NMR. To assess compounds $\mathbf{2}^{\mathbf{Mes}}$ and $\mathbf{2}^{\mathbf{Dipp}}$ as potential precursors for Ni–B bonded species, they were each reacted with one

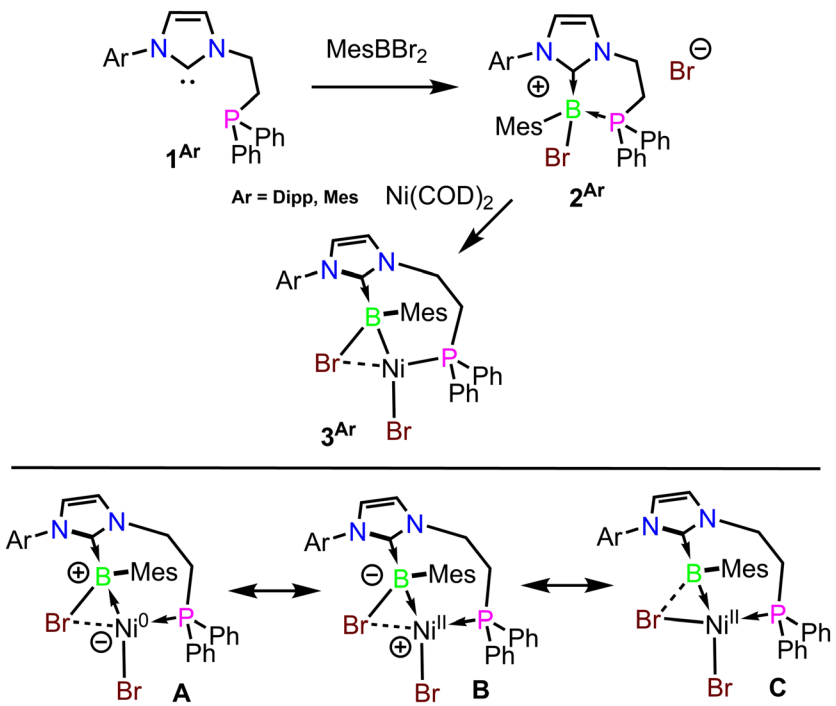

Scheme 1 Synthesis of the Ni–B complexes $\mathbf{3}^{\mathbf{Mes}}$ and $\mathbf{3}^{\mathbf{Dipp}}$ (top) and possible resonance contributors (bottom).

equivalent of $Ni(COD)_2$ at ambient temperature. A colour change to dark purple was observed in both reactions over the course of 30 minutes, and upon workup the compounds $\mathbf{3^{Mes}}$ and $\mathbf{3^{Dipp}}$ were isolated in 58% and 52% yields, respectively, as diamagnetic dark purple solids (Scheme 1). Single crystals of $\mathbf{3^{Dipp}}$ were obtained, and an X-ray diffraction study revealed a surprising structure featuring a newly formed Ni–B bond with highly distorted coordination environments at both Ni and B. Addition of one B–Br moiety to Ni has occurred completely, while the other bromide remains bridged through both Ni and B centres, forming a highly distorted square planar geometry at Ni (Fig. 2). The $B–Br_{(bridging)}$ and $Ni–Br_{(bridging)}$ bond lengths are 2.087(8) Å and 2.393(1) Å, respectively, both of which are in the characteristic range of single bonds. The Ni–B distance is 2.008(8) Å, which is somewhat longer than those typically observed in borylnickel complexes (typically 1.90–1.95 Å),[10,11,14,28–30] but shorter than those observed in Ni → BAr_3 complexes (2.10–2.35 Å).[17] The geometry of the 4-coordinate boron centre is also distorted where the sum of the bond angles involving C_{NHC}, C_{Mes} and Ni atoms is close to planar (350.3°), reminiscent of singly base-stabilized metalloborylenes[61–63] and initially suggestive of an electrostatic interaction between the bridging bromide and boron. Anagostic interactions[64] are also present between the Ni centre and a mesityl-CH_3 group with a bond length of 2.238 Å, and to a methine position of the Dipp group with a bond length of 2.908 Å. A corresponding downfield-shifted and broadened resonance at 3.27 ppm in the ^1H NMR (THF-D_8) is observed for the mesityl CH_3 group. ^{11}B NMR resonances of 9.8 and 8.2 ppm were observed for $\mathbf{3^{Mes}}$ and $\mathbf{3^{Dipp}}$ in THF-D_8, respectively, and $^{31}P\{^1H\}$ NMR indicates coordination of the phosphorus centre to Ni, with resonances observed at 21.8 and 20.9 ppm, respectively. Both compounds are decomposed by DMSO or halogenated solvents, and are also highly sensitive to air both in the solid state and in solution.

To gain insight on the electronic structure of these species, DFT calculations were performed on $\mathbf{3^{Dipp}}$ (PBE0-D3(BJ)/Def2TZVP). The choice of this particular level of theory was based on its successful application in several recently studied low-valent Ni and borylnickel systems[11,32,65] and its excellent reproduction of the metric parameters of the experimental crystal structure of $\mathbf{3^{Dipp}}$. Furthermore, the employed level of theory gives also excellent descriptions of valence and core-level excited states of $\mathbf{3^{Dipp}}$ (*vide infra*). Given the presence of the bridging bromide anion, we first became curious on the nature of its bonding interactions with nickel and boron. Mayer bond order (MBO) calculations indicate a markedly lower bond order between Ni and the bridging bromide (MBO = 0.51), than to the terminal bromide (MBO = 0.72). Strong bonding interactions are present between Ni–B (MBO = 0.67), and B–Br (MBO = 0.77). To gain further insight on the bonding environment around the nickel center, QTAIM analysis of the Laplacian of electron density was performed on $\mathbf{3^{Dipp}}$. Bond critical points were identified between $Ni–Br_{(terminal)}$ ($\rho(r)$ = 0.07 a.u.; $H(r)$ = −0.02 a.u.; $\nabla^2\rho(r)$ = 0.18 a.u.), Ni–P ($\rho(r)$ = 0.11 a.u.; $H(r)$ = −0.06 a.u.; $\nabla^2\rho(r)$ = 0.14 a.u) and Ni–B ($\rho(r)$ = 0.09 a.u.; $H(r)$ = −0.04 a.u.; $\nabla^2\rho(r)$ = −0.01 a.u.), indicative of covalent/donor–acceptor bonding between Ni–B and non-covalent interactions dominating between $Ni–Br_{(terminal)}$, and Ni–P. Notably, this analysis indicates the striking absence of a bond critical point between Ni and the bridging bromide, suggesting a predominantly coulombic interaction with a low degree of electron sharing between these two atoms (Fig. 3a). Upon analysing the electron density difference contour plots (Fig. S29) we observe very different behaviour of the bridging and terminal bromides. When considering the changes in electron density when adding each bromide to the metal centre, the $Ni–Br_{(terminal)}$ bond reveals a characteristic

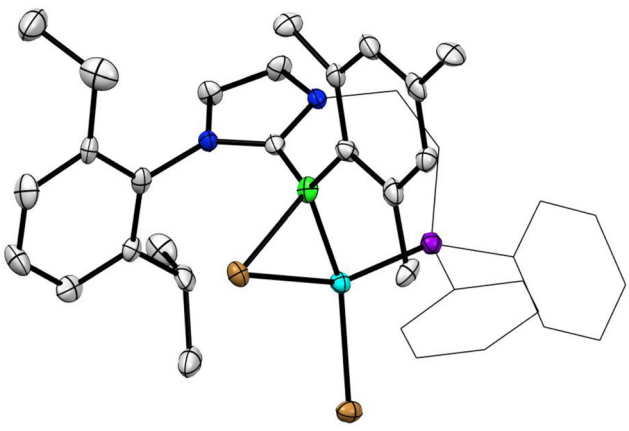

Fig. 2 Molecular structure of $\mathbf{3^{Dipp}}$. Thermal ellipsoids are drawn at 50% probability. Hydrogen atoms are removed for clarity. Aryl/alkyl substituents on phosphorus are drawn as wireframe for clarity. Colours: boron; lime green, carbon; grey, nitrogen; blue, phosphorus; purple, nickel; teal, bromine; brown. Selected bond lengths (Å) and angles (°): B–Br; 2.087(8), B–Ni; 2.008(8), $B–C_{NHC}$; 1.592(11), $B–C_{Mes}$; 1.603(10), $Ni–Br_{(bridging)}$; 2.393(1), $Ni–Br_{(terminal)}$; 2.390(1), Ni–P; 2.121(2). $C_{NHC}–B–C_{Mes}$; 122.1(6), $C_{Mes}–B–Ni$: 125.8(5); $C_{NHC}–B–Ni$: 102.4(4), $C_{Mes}–B–Br$; 112.6(5), $C_{NHC}–B–Br$; 111.7(5), Ni–B–Br; 71.5(3), $P–Ni–Br_{(terminal)}$; 101.87(6), Br–Ni–Br; 102.12(4), $Br_{(bridging)}–Ni–B$; 55.8(2), B–Ni–P; 100.1(2); $B–Br_{(bridging)}–Ni$; 52.7(2).

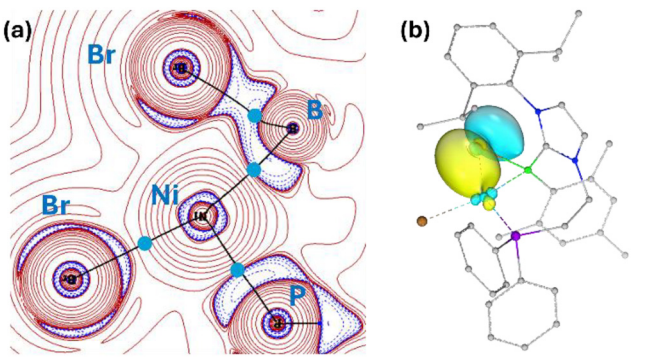

Fig. 3 (a) QTAIM analysis of the Laplacian of electron density of $\mathbf{3^{Dipp}}$, viewed in the plane of the Ni–Br/B–Br nickel bonding environment. Bond critical points are highlighted in blue. (b) IBO involving Ni and the bridging Br anion (89% Br, 6% Ni).

loss of electron density from both the Ni and Br centres and the emergence of electron density along the bond path, as is typical. However, in the case of the bridging bromide, electron density difference can only be described as polarization of each atomic centre without the formation of a clear region of increased electron density corresponding to this interaction. At the same time, a similar electron density difference contours are visible along the B–Br bond as for the terminal Br–Ni bond. Additionally, the Ni–$Br_{(bridging)}$ Intrinsic Bond Orbital (IBO) is essentially an unhybridized 4p orbital of bromide, with only a minor contribution from the Ni centre (89% Br, 6% Ni) (Fig. 3b). Whereas in the interaction of boron with the bridging bromide, the B–Br IBO is a hybrid orbital (31% B, 67% Br) (Fig. 3a and S27). Collectively, this data suggests that the B-ligand in $\mathbf{3^{Dipp}}$ is not a borylene (Scheme 1C), but rather a boryl-type [(NHC)B(Mes)Br] ligand supported by an electrostatic Br–Ni interaction (Scheme 1A and B). Bond critical points are also observed in the Ni···H_3C_{Mes} and Ni···HC_{Dipp} anagostic interactions (Fig. S28 and Table S2).

The Ni–B bonding interaction is present in the HOMO and involves the greatest contribution from the metal centre (37% Ni, 22% Br, 14% B) (Fig. 4a). The Ni–B IBO indicates a highly covalent interaction between the two centres, which is also slightly delocalized through the vacant 2p orbital on the adjacent carbene carbon (53% Ni, 38% B, 6% C) (Fig. 4c). The LUMO is highly delocalized but is primarily ligand-centred. It features π orbital encompassing both the boron and the carbene–carbon centres and an antibonding interaction of this with the Ni centre (23% B, 12% Ni) (Fig. 4b). These interactions (metal-centred bonding HOMO, ligand-centred antibonding LUMO) are observed in complexes featuring M→Z donor/acceptor interactions and are a hallmark of complexes with an inverted ligand field.[66–69]

To probe the effective oxidation state of the nickel centre in $\mathbf{3^{Dipp}}$ experimentally, we conducted complementary XANES measurements at the metal K- and L-edges of $\mathbf{3^{Dipp}}$ as well as reference compounds NiF_2, $NiCl_2$, Ni metal, and $[Et_4N]_2[NiCl_4]$. The metal K-edge features are formed by the excitation of the core Ni 1s electron into the frontier unoccupied orbitals below the ionization threshold. Due to the dipole-allowed nature of XAS excitations, intense peaks are observed for the Ni 1s→4p transitions, which determine the rising-edge spectral features. The rising-edge inflection points (Fig. 5a – marked by enlarged diamond symbols) can be correlated with the effective nuclear charge experienced by the excited 1s core electron, and the effective oxidation state of the metal absorber. The ionization energy of metallic Ni(0) was calibrated to 8333.0 eV (black trace). From this analysis, NiF_2 is the least covalent Ni(II) compound featuring an inflection point shifted 11.7 eV higher in energy due to the increased nuclear charge at the Ni centre. Increased metal–ligand covalency and a reduction of the

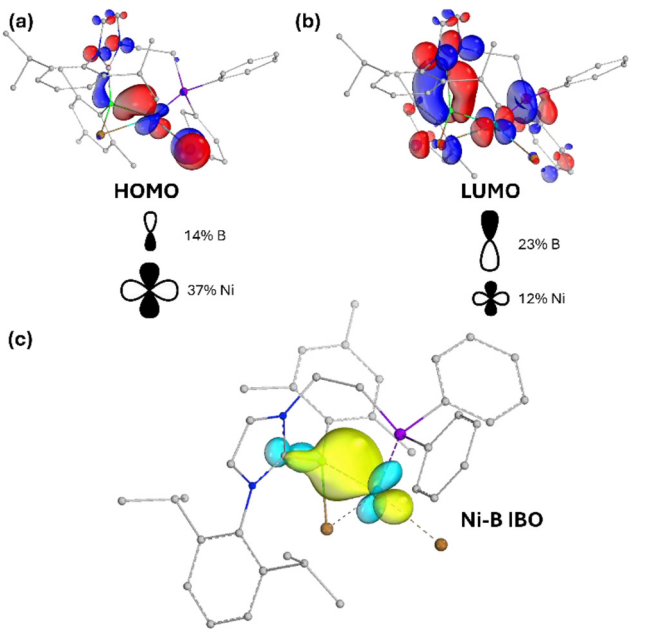

Fig. 4 (a) HOMO of $\mathbf{3^{Dipp}}$. (b) LUMO of $\mathbf{3^{Dipp}}$. (c) Nickel–boron IBO (53% Ni, 38% B, 6% $C_{carbene}$).

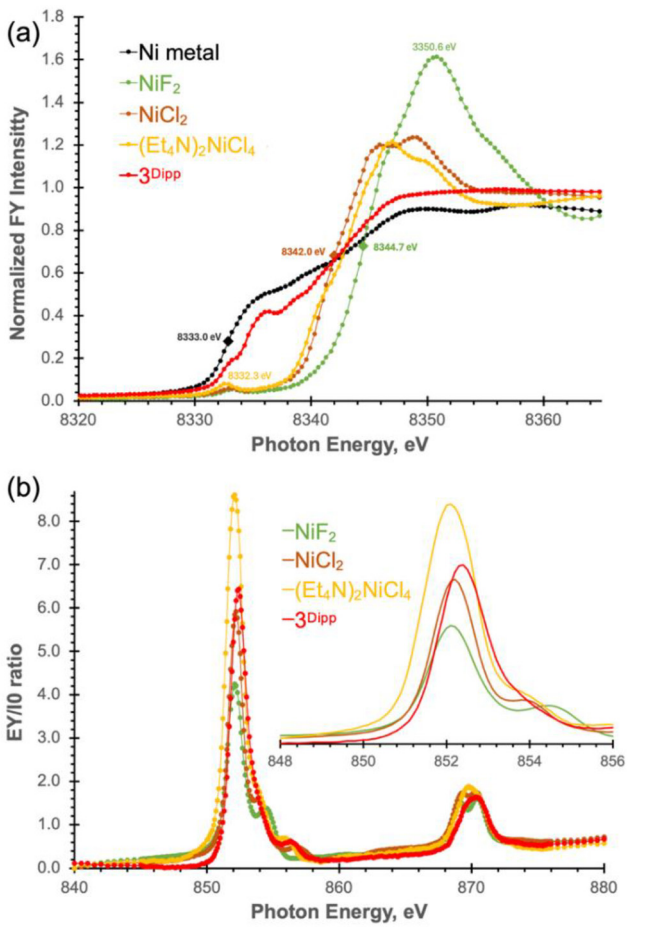

Fig. 5 X-ray absorption near-edge spectra at the Ni K-edge (a) and Ni L-edges (b) for reference compounds Ni metal foil, NiF_2, $NiCl_2$, and $(Et_4N)_2NiCl_4$ with well-defined electronic and geometric structures and $\mathbf{3^{Dipp}}$.

effective oxidation state of the nickel is observed in $NiCl_2$ and $[Et_4N]_2[NiCl_4]$, as indicated by the −2.7 eV shift in energy of the rising-edge inflection point, with respect to NiF_2 (golden and brown traces). The higher covalency in the tetrahedral complex cannot be directly derived from the metal K-edge spectrum given the ambiguity of the rising-edge inflection point; however, this is clearly demonstrated by the complementary Cl K-edge spectra in the tender X-ray energy range with a more intense pre-edge feature for the former (Fig. S23). The Ni K-edge spectrum of $\mathbf{3^{Dipp}}$ (Fig. 5a, red trace) leaves no uncertainty in the absorber's effective charge given its close proximity to the metallic Ni(0) spectrum. The positive energy shift from the Ni(0) foil spectrum is due to Ni→B/NHC backdonation, which gives rise to at least two shoulders along the rising-edge at 8333.2 and 8336.4 eV.

In moving from the hard X-ray energy range of Ni K-edge to the soft X-ray energy region, the excitations of the Ni 2p core electrons give rise to the Ni L-edge spectra (Fig. 5b). Due to the significant charging effects and varied conductivity of the samples, the peak intensities do not follow the expected complementary covalency changes from the Cl and Ni K-edge measurements; however, the excitation energy peak positions are informative as shown for the L_3 energy region (Fig. 5b, inset). The smallest ligand field splitting and thus the lowest excitation energy is observed for the $[NiCl_4]^{2-}$ at 852.0 eV. The competition between Ni–Cl bond covalency and ligand field strength gives close to identical Ni 2p→3d main excitation peaks (852.2 eV) at the L_3 edge for NiF_2 and $NiCl_2$. The highest energy transition is clearly observed for the most reduced Ni centre in $\mathbf{3^{Dipp}}$ (red trace), and is to the frontier unoccupied orbitals that are outside of the 3d-manifold range at 852.4 eV. The corresponding rising-edge feature for metallic Ni L_3-edge is at 852.7 eV (calibration point). Due to the asymmetric shape of the red trace, three excitations can be assigned based on electronic structure calculations. Time-dependent DFT (PBE0-D3(BJ)/QZ4P) calculations identify three well-resolved excitations for the Ni K- and L-edges (Fig. S30 and S31). While the donor orbitals for the excitations originate from 1s at the K-edge and 2p at the L-edge, the acceptor orbitals are identical. These are the LUMO (Fig. 4b), the LUMO+2 (mixed NHC, B, and minor Ni 3d orbital contributions), and the LUMO+14 (mixture of NHC C/N 2p, H 1s, and minor Ni 3d contributions) (Fig. S33 and Table S5). In support of the self-consistency of the ground and excited state descriptions by the selected functional, we have also found excellent reproduction of the UV-Vis spectrum of $\mathbf{3^{Dipp}}$ (Fig. S32), where the acceptor orbitals in the valence-level excitations are the same as for the core-level excitations described above.

Collectively, these data confirm a low-valent Ni centre in $\mathbf{3^{Dipp}}$. In further support of this, NBO analysis indicates an electronic configuration of $4s^{0.34}3d^{9.26}$ for the Ni centre in $\mathbf{3^{Dipp}}$, suggesting a somewhat *greater* d orbital population than the recently reported Ni(0)–borane complex by Hoshimoto and coworkers (Fig. 1D).[38] Additionally, effective oxidation state (EOS) calculations[70] also indicate that $\mathbf{3^{Dipp}}$ is best formulated as a Ni(0)/B(III) system with an 87% figure of confidence. Finally, density of state (DOS) calculations also lend further credence to the assignment of Ni(0) in $\mathbf{3^{Dipp}}$, where there is clearly minimal d orbital density associated with frontier unoccupied molecular orbitals (Fig. S34). This is contrasted with a Ni(I)–borane complex reported by Peters' and coworkers,[9] where the electron hole in the d shell is evidenced by significant d density within the LUMO. From all this analysis collectively, it is clear that $\mathbf{3^{Dipp}}$ is best described as a Ni(0)/B(III) complex (Scheme 1A), implying that with $[(NHC)BR_2]$-type ligands a Z-type bonding interaction may be preferred with electronegative metals such as nickel.

Next, we examined the reactivity of these highly covalent Ni–B bonded complexes. Compounds $\mathbf{3^{Dipp}}$/$\mathbf{3^{Mes}}$ are both highly sensitive and react unselectively in the presence of nucleophiles such as pyridine, DMAP, CO, nitriles, H_2, as well as reducing agents such as KC_8 and $Na_2[Fe(CO)_4]$. In all of these reactions no products could be isolated. However, a selective reaction was observed with an isocyanide, where combination of $\mathbf{3^{Dipp}}$ in THF with an equimolar amount of 4-meth-

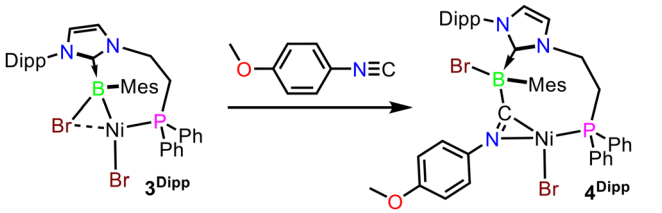

Scheme 2 Insertion of an isonitrile to form the metallobicycle $\mathbf{4^{Dipp}}$.

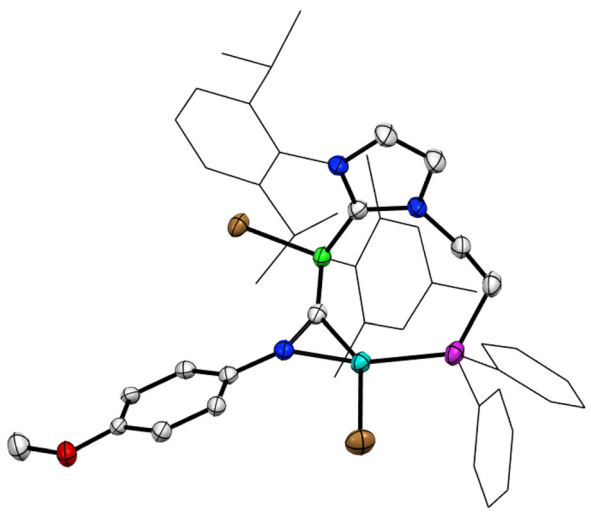

Fig. 6 Molecular structure of $\mathbf{4^{Dipp}}$. Thermal ellipsoids are drawn at 50% probability. Hydrogen atoms are removed for clarity. Aryl substituents on phosphorus and the Dipp/Mes groups are drawn as wireframe for clarity. Colours: boron; lime green, carbon; grey, nitrogen; blue, oxygen; red, phosphorus; purple, nickel; teal, bromine; brown. Selected bond lengths (Å) and angles (°): Ni–Br: 2.3583(5), Ni–P: 2.1451(8), Ni–N: 1.859(2), Ni–C: 1.879(3), $C_{nitrile}$–N: 1.389(5), B–C: 1.628(4), B–Br: 2.078 (3), P–Ni–Br: 97.38(3), Br–Ni–N: 108.21(7), N–Ni–C: 39.26(11), C–Ni–P: 114.71(9).

oxyphenylisocyanide resulted in an immediate darkening of the reaction mixture. ^{11}B NMR revealed the formation of a single new product with a very broad resonance at −12.4 ppm, and single crystals of green–yellow $\mathbf{4^{Dipp}}$ could be isolated in a 46% yield *via* layering of the reaction mixture with pentane (Scheme 2). A single crystal X-ray diffraction study revealed $\mathbf{4^{Dipp}}$ to be derived from insertion of the isocyanide carbon into the Ni–B bond, forming a metallobicyclo[6.1.0]nonane structure (Fig. 6). The nickel centre adopts a distorted trigonal planar coordination environment, where both the boron and nickel centres each retain one bromide ligand. To our knowledge, compound $\mathbf{4^{Dipp}}$ is the first example of an isocyanide insertion into a metal–boron bond with the formation of a M–N–C three-membered metallocycle, as B–N bond formation and/or monodentate coordination of the isocyanide carbon is typically observed in these insertion reactions.[71,72]

We have also examined the suitability of B–Cl bonds for the construction of nickel–boron bonds in analogous addition reactions to Ni(COD)$_2$. The adduct $\mathbf{5^{Mes}}$ was prepared from a reaction between the free carbene $\mathbf{1^{Mes}}$ and MesBCl$_2$ (see SI).

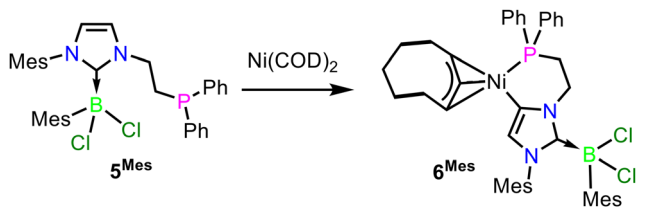

Scheme 3 Reaction of the chloride analogue $\mathbf{5^{Mes}}$ to form a Ni-abnormal carbene $\mathbf{6^{Mes}}$.

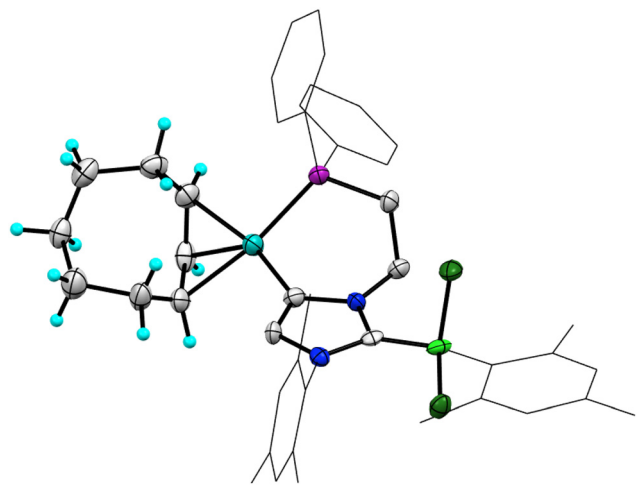

Fig. 7 Molecular structure of $\mathbf{6^{Mes}}$. Thermal ellipsoids are drawn at 50% probability. Hydrogen atoms, except those on the η^3-C_8H_{13} ligand, are removed for clarity. Aryl substituents on phosphorus and the Mes groups are drawn as wireframe for clarity. Colours: hydrogen; sky blue, boron; lime green, carbon; grey, nitrogen; blue, chlorine; forest green, phosphorus; purple, nickel; teal. Selected bond lengths (Å) and angles (°): Ni–C_{NHC}: 1.914(6), Ni–P: 2.1555(19), Ni–C_{allyl}: 2.073(7), 2.074(7), 1.964(7), B–C: 1.626(10). P–Ni–C_{NHC}: 96.6(2).

When combined with Ni(COD)$_2$ in benzene, the mixture rapidly became deep yellow, and upon the addition of pentane a yellow solid was obtained (Scheme 3). Recrystallization from toluene/pentane afforded single crystals of the product $\mathbf{6^{Mes}}$ suitable for X-ray diffraction in a 45% yield (Scheme 3). The molecular structure revealed that rather than B–Cl addition, C–H activation of the C4 position of the imidazole-2-ylidene had occurred, concomitant with hydride transfer to the COD ligand forming an η^3-allyl complex and an abnormally-bound anionic carbene ligand (Fig. 7).[73] Similar C4- and C5-bound imidazol-2-ylidene nickel complexes have recently been explored for their catalytic activity in heteroarylation and nitroarene reduction reactions.[74–77] The formation of a similar complex here indicates that B–Cl addition presents a more significant kinetic barrier than ligand C–H activation, and that the use of bromoborane ligands will likely be necessary for the construction of larger families of Ni–B bonded systems.

Conclusions

In summary, we have prepared the first examples of NHC-supported boryl complexes of nickel, and have demonstrated that they possess significant Ni(0) character where the boron ligand accepts electron density from Ni as a Z-type ligand. The Ni K- and L-edge spectra are in unambiguous agreement with ground and excited state hybrid density functional calculations on the effective Ni(0) oxidation state for the metal with significant donation to the B(III) and NHC ligands. Reactivity studies have indicated the necessity of a bromoborane precursor in the construction of these complexes and have found an unprecedented insertion reaction of the isocyanide to the Ni–B bond. The application of this ligand type to bond activation and catalysis are ongoing in our laboratory.

Author contributions

YX. W., E. M., and C. P. synthesized and characterized all complexes, including the collection of single crystal XRD data. V. P. and J. W. performed the DFT calculations. R. K. Sz. collected and analysed the XAS data and assisted in the interpretation of electronic structure analysis. C. P. conceived and supervised the study, solved the XRD data, and wrote the manuscript with input from all authors.

Conflicts of interest

There are no conflicts to declare.

Data availability

Data supporting the conclusions of this manuscript, along with all experimental details can be found in the supplementary information (SI). Supplementary information: experi-

mental & computational details. See DOI: https://doi.org/10.1039/d5qi02109j.

CCDC 2492761–2492765 and 2493820 contain the supplementary crystallographic data for this paper.[78a–f]

Acknowledgements

C. P. thanks the Digital Research Alliance of Canada and The University of British Columbia's Advanced Research Computing for computing facilities. C. P. acknowledges NSERC Discovery Grant RGPIN-2021-03056 and CFI JELF/BCKDF 41570 for funding. R. K. Sz. is thankful for the use of the Stanford Synchrotron Radiation Lightsource, SLAC National Accelerator Laboratory, which is supported by the U. S. Department of Energy, Office of Science, Office of Basic Energy Sciences under Contract No. DE-AC02-76SF00515.

References

1 B. Marciniec, C. Pietraszuk, P. Pawluć and H. Maciejewski, Inorganometallics (Transition Metal–Metalloid Complexes) and Catalysis, *Chem. Rev.*, 2022, **122**(3), 3996–4090.
2 J. Zhou, M. W. Kuntze-Fechner, R. Bertermann, U. S. D. Paul, J. H. J. Berthel, A. Friedrich, Z. Du, T. B. Marder and U. Radius, Preparing (Multi)Fluoroarenes as Building Blocks for Synthesis: Nickel-Catalyzed Borylation of Polyfluoroarenes via C–F Bond Cleavage, *J. Am. Chem. Soc.*, 2016, **138**(16), 5250–5253.
3 Y.-M. Tian, X.-N. Guo, M. W. Kuntze-Fechner, I. Krummenacher, H. Braunschweig, U. Radius, A. Steffen and T. B. Marder, Selective Photocatalytic C–F Borylation of Polyfluoroarenes by Rh/Ni Dual Catalysis Providing Valuable Fluorinated Arylboronate Esters, *J. Am. Chem. Soc.*, 2018, **140**(50), 17612–17623.
4 L. Kuehn, D. G. Jammal, K. Lubitz, T. B. Marder and U. Radius, Stoichiometric and Catalytic Aryl–Cl Activation and Borylation using NHC-stabilized Nickel(0) Complexes, *Chem. – Eur. J.*, 2019, **25**(40), 9514–9521.
5 Y.-M. Tian, X.-N. Guo, I. Krummenacher, Z. Wu, J. Nitsch, H. Braunschweig, U. Radius and T. B. Marder, Visible-Light-Induced Ni-Catalyzed Radical Borylation of Chloroarenes, *J. Am. Chem. Soc.*, 2020, **142**(42), 18231–18242.
6 Y.-M. Tian, X.-N. Guo, Z. Wu, A. Friedrich, S. A. Westcott, H. Braunschweig, U. Radius and T. B. Marder, Ni-Catalyzed Traceless, Directed C_3-Selective C–H Borylation of Indoles, *J. Am. Chem. Soc.*, 2020, **142**(30), 13136–13144.
7 Y.-M. Tian, X.-N. Guo, H. Braunschweig, U. Radius and T. B. Marder, Photoinduced Borylation for the Synthesis of Organoboron Compounds, *Chem. Rev.*, 2021, **121**(7), 3561–3597.
8 S. K. Bose, L. Mao, L. Kuehn, U. Radius, J. Nekvinda, W. L. Santos, S. A. Westcott, P. G. Steel and T. B. Marder, First-Row d-Block Element-Catalyzed Carbon–Boron Bond Formation and Related Processes, *Chem. Rev.*, 2021, **121**(21), 13238–13341.
9 W. H. Harman and J. C. Peters, Reversible H2 Addition across a Nickel–Borane Unit as a Promising Strategy for Catalysis, *J. Am. Chem. Soc.*, 2012, **134**(11), 5080–5082.
10 T.-P. Lin and J. C. Peters, Boryl–Metal Bonds Facilitate Cobalt/Nickel-Catalyzed Olefin Hydrogenation, *J. Am. Chem. Soc.*, 2014, **136**(39), 13672–13683.
11 P. Ríos, J. Borge, F. Fernández de Córdova, G. Sciortino, A. Lledós and A. Rodríguez, Ambiphilic boryl groups in a neutral Ni(ii) complex: a new activation mode of H_2, *Chem. Sci.*, 2021, **12**(7), 2540–2548.
12 Z. Chen, H. Liang, J. Lin, Y. Liu, Y. Li and Z. Ke, Distinct electronic effects of borane– and boryl–nickel complexes for catalyzing H_2 activation, *Inorg. Chem. Front.*, 2023, **10**(23), 6928–6935.
13 F. Kong, P. Ríos, C. Hauck, F. J. Fernández-de-Córdova, D. A. Dickie, L. G. Habgood, A. Rodríguez and T. B. Gunnoe, Ethylene Dimerization and Oligomerization Using Bis(phosphino)boryl Supported Ni Complexes, *J. Am. Chem. Soc.*, 2023, **145**(1), 179–193.
14 F. W. Seidel and K. Nozaki, A Ni^0 σ-Borane Complex Bearing a Rigid Bidentate Borane/Phosphine Ligand: Boryl Complex Formation by Oxidative Dehydrochloroborylation and Catalytic Activity for Ethylene Polymerization, *Angew. Chem., Int. Ed.*, 2022, **61**(6), e202111691.
15 L. Álvarez-Rodríguez, P. Ríos, C. J. Laglera-Gándara, A. Jurado, F. J. Fernández-de-Córdova, T. B. Gunnoe and A. Rodríguez, Cleavage of Carbon Dioxide C=O Bond Promoted by Nickel-Boron Cooperativity in a PBP-Ni Complex, *Angew. Chem., Int. Ed.*, 2023, **62**(34), e202306315.
16 A. Amgoune and D. Bourissou, σ-Acceptor, Z-type ligands for transition metals, *Chem. Commun.*, 2011, **47**(3), 859–871.
17 H. Braunschweig and R. D. Dewhurst, Transition metals as Lewis bases: "Z-type" boron ligands and metal-to-boron dative bonding, *Dalton Trans.*, 2011, **40**(3), 549–558.
18 H. Braunschweig, R. D. Dewhurst and A. Schneider, Electron-Precise Coordination Modes of Boron-Centered Ligands, *Chem. Rev.*, 2010, **110**(7), 3924–3957.
19 X. Guo and Z. Lin, Boryls, their compounds and reactivity: a structure and bonding perspective, *Chem. Sci.*, 2024, **15**(9), 3060–3070.
20 H. Kameo and H. Nakazawa, Recent Developments in the Coordination Chemistry of Multidentate Ligands Featuring a Boron Moiety, *Chem. – Asian J.*, 2013, **8**(8), 1720–1734.
21 G. J. Irvine, M. J. G. Lesley, T. B. Marder, N. C. Norman, C. R. Rice, E. G. Robins, W. R. Roper, G. R. Whittell and L. J. Wright, Transition Metal–Boryl Compounds: Synthesis, Reactivity, and Structure, *Chem. Rev.*, 1998, **98**(8), 2685–2722.
22 L. Dang, Z. Lin and T. B. Marder, Boryl ligands and their roles in metal-catalysed borylation reactions, *Chem. Commun.*, 2009, (27), 3987–3995.
23 J. Zhu, Z. Lin and T. B. Marder, Trans Influence of Boryl Ligands and Comparison with C, Si, and Sn Ligands, *Inorg. Chem.*, 2005, **44**(25), 9384–9390.

24 K. C. Lam, W. H. Lam, Z. Lin, T. B. Marder and N. C. Norman, Structural Analysis of Five-Coordinate Transition Metal Boryl Complexes with Different d-Electron Configurations, *Inorg. Chem.*, 2004, **43**(8), 2541–2547.
25 H. Braunschweig, B. Christ, M. Colling-Hendelkens, M. Forster, K. Götz, M. Kaupp, K. Radacki and F. Seeler, Synthesis, Structure, and Bonding of Novel Homodinuclear Cobalt and Nickel Borylene Complexes, *Chem. – Eur. J.*, 2009, **15**(29), 7150–7155.
26 B. B. Macha, D. Dhara, K. Radacki, R. D. Dewhurst and H. Braunschweig, Intermetallic transfer of unsymmetrical borylene fragments: isolation of the second early-transition-metal terminal borylene complex and other rare species, *Dalton Trans.*, 2020, **49**(48), 17719–17724.
27 T. J. Hadlington, T. Szilvási and M. Driess, Silylene–Nickel Promoted Cleavage of B–O Bonds: From Catechol Borane to the Hydroborylene Ligand, *Angew. Chem., Int. Ed.*, 2017, **56**(26), 7470–7474.
28 D. Adhikari, J. C. Huffman and D. J. Mindiola, Structural elucidation of a nickel boryl complex. A recyclable borylation Ni(ii) reagent of bromobenzene, *Chem. Commun.*, 2007, (43), 4489–4491.
29 B. L. Tran, D. Adhikari, H. Fan, M. Pink and D. J. Mindiola, Facile entry to 3d late transition metal boryl complexes, *Dalton Trans.*, 2010, **39**(2), 358–360.
30 N. Curado, C. Maya, J. López-Serrano and A. Rodríguez, Boryl-assisted hydrogenolysis of a nickel–methyl bond, *Chem. Commun.*, 2014, **50**(99), 15718–15721.
31 G. Audsley, A. Carpentier, A.-F. Pécharman, J. Wright, T. M. Roseveare, E. R. Clark, S. A. Macgregor and I. M. Riddlestone, Contrasting reactivity of B–Cl and B–H bonds at $[Ni(IMes)_2]$ to form unsupported Ni-boryls, *Chem. Commun.*, 2024, **60**(7), 874–877.
32 L. Tendera, F. Fantuzzi, T. B. Marder and U. Radius, Nickel boryl complexes and nickel-catalyzed alkyne borylation, *Chem. Sci.*, 2023, **14**(8), 2215–2228.
33 L. Tendera, L. Kuehn, T. B. Marder and U. Radius, On the Reactivity of a NHC Nickel Bis-Boryl Complex: Reductive Elimination and Formation of Mono-Boryl Complexes, *Chem. – Eur. J.*, 2023, **29**(62), e202302310.
34 J. R. Prat, R. C. Cammarota, B. J. Graziano, J. T. Moore and C. C. Lu, Toggling the Z-type interaction off-on in nickel-boron dihydrogen and anionic hydride complexes, *Chem. Commun.*, 2022, **58**(63), 8798–8801.
35 M. Sircoglou, S. Bontemps, G. Bouhadir, N. Saffon, K. Miqueu, W. Gu, M. Mercy, C.-H. Chen, B. M. Foxman, L. Maron, O. V. Ozerov and D. Bourissou, Group 10 and 11 Metal Boratranes (Ni, Pd, Pt, CuCl, AgCl, AuCl, and Au^+) Derived from a Triphosphine–Borane, *J. Am. Chem. Soc.*, 2008, **130**(49), 16729–16738.
36 W. H. Harman, T.-P. Lin and J. C. Peters, A d^{10} Ni–(H_2) Adduct as an Intermediate in H-H Oxidative Addition across a Ni-B Bond, *Angew. Chem., Int. Ed.*, 2014, **53**(4), 1081–1086.
37 B. E. Cowie and D. J. H. Emslie, Nickel and Palladium Complexes of Ferrocene-Backbone Bisphosphine-Borane and Trisphosphine Ligands, *Organometallics*, 2015, **34**(16), 4093–4101.
38 Y. Mondori, Y. Yamauchi, T. Kawakita, S. Ogoshi, Y. Uetake, Y. Takeichi, H. Sakurai and Y. Hoshimoto, Monodentate σ-Accepting Boron-Based Ligands Bearing Square-Planar Ni(0) Centers, *J. Am. Chem. Soc.*, 2025, **147**(10), 8326–8335.
39 H. Kameo, Y. Tanaka, Y. Shimoyama, D. Izumi, H. Matsuzaka, Y. Nakajima, P. Lavedan, A. Le Gac and D. Bourissou, Square-Planar Anionic Pt^0 Complexes, *Angew. Chem., Int. Ed.*, 2023, **62**(20), e202301509.
40 M. Sircoglou, S. Bontemps, M. Mercy, N. Saffon, M. Takahashi, G. Bouhadir, L. Maron and D. Bourissou, Transition-Metal Complexes Featuring Z-Type Ligands: Agreement or Discrepancy between Geometry and dn Configuration?, *Angew. Chem., Int. Ed.*, 2007, **46**(45), 8583–8586.
41 Y. Segawa, M. Yamashita and K. Nozaki, Boryllithium: Isolation, Characterization, and Reactivity as a Boryl Anion, *Science*, 2006, **314**(5796), 113–115.
42 H. M. Hansen, P. Garg, J. J. Schuely, M. Y. Yang, O. K. Farha, J. M. Keith and S. R. Daly, Flash Communication: Boron K-edge XAS and TDDFT Studies of Covalent Metal–Ligand Bonding in $Ni(C_2B_9H_{11})_2$, *Organometallics*, 2025, **44**(15), 1624–1629.
43 V. Nesterov, D. Reiter, P. Bag, P. Frisch, R. Holzner, A. Porzelt and S. Inoue, NHCs in Main Group Chemistry, *Chem. Rev.*, 2018, **118**(19), 9678–9842.
44 B. Borthakur, B. Ghosh and A. K. Phukan, The flourishing chemistry of carbene stabilized compounds of group 13 and 14 elements, *Polyhedron*, 2021, **197**, 115049.
45 D. P. Curran, A. Solovyev, M. Makhlouf Brahmi, L. Fensterbank, M. Malacria and E. Lacôte, Synthesis and Reactions of N-Heterocyclic Carbene Boranes, *Angew. Chem., Int. Ed.*, 2011, **50**(44), 10294–10317.
46 X. Mao, S. Qiu, R. Guo, Y. Dai, J. Zhang, L. Kong and Z. Xie, Cyclic (Alkyl)(Amino)Carbene-Iminoboryl Compounds with Three Formal Oxidation States, *J. Am. Chem. Soc.*, 2024, **146**(15), 10917–10924.
47 W. Kennedy, V. Pattathil, Y. Wei, F. Fantuzzi and C. Pranckevicius, Ambient Temperature Isolation of a Monatomic Boron(0) Complex, *J. Am. Chem. Soc.*, 2025, **147**(4), 3500–3506.
48 T. Heitkemper and C. P. Sindlinger, A Cationic NHC-Supported Borole, *Chem. – Eur. J.*, 2020, **26**(51), 11684–11689.
49 G. Kundu, P. R. Amrutha, S. Tothadi and S. S. Sen, Saturated NHC-Stabilized Borenium, Boronium, Hydride-Bridged Boron Cations, and a Bora-Acyl Chloride, *Organometallics*, 2024, **43**(12), 1355–1361.
50 J. M. Farrell, J. A. Hatnean and D. W. Stephan, Activation of Hydrogen and Hydrogenation Catalysis by a Borenium Cation, *J. Am. Chem. Soc.*, 2012, **134**(38), 15728–15731.
51 J. M. Farrell, R. T. Posaratnanathan and D. W. Stephan, A family of N-heterocyclic carbene-stabilized borenium ions for metal-free imine hydrogenation catalysis, *Chem. Sci.*, 2015, **6**(3), 2010–2015.

52 G. Kundu, K. Balayan, S. Tothadi and S. S. Sen, Six-Membered Saturated NHC-Stabilized Borenium Cations: Isolation of a Cationic Analogue of Borinic Acid, *Inorg. Chem.*, 2022, **61**(33), 12991–12997.
53 M. F. Silva Valverde, P. Schweyen, D. Gisinger, T. Bannenberg, M. Freytag, C. Kleeberg and M. Tamm, N-Heterocyclic Carbene Stabilized Boryl Radicals, *Angew. Chem., Int. Ed.*, 2017, **56**(4), 1135–1140.
54 T. Taniguchi, Advances in chemistry of N-heterocyclic carbene boryl radicals, *Chem. Soc. Rev.*, 2021, **50**(16), 8995–9021.
55 H. Braunschweig, C.-W. Chiu, K. Radacki and T. Kupfer, Synthesis and Structure of a Carbene-Stabilized π-Boryl Anion, *Angew. Chem., Int. Ed.*, 2010, **49**(11), 2041–2044.
56 J. Monot, A. Solovyev, H. Bonin-Dubarle, É. Derat, D. P. Curran, M. Robert, L. Fensterbank, M. Malacria and E. Lacôte, Generation and Reactions of an Unsubstituted N-Heterocyclic Carbene Boryl Anion, *Angew. Chem., Int. Ed.*, 2010, **49**(48), 9166–9169.
57 R. Böser, L. C. Haufe, M. Freytag, P. G. Jones, G. Hörner and R. Frank, Completing the series of boron-nucleophilic cyanoborates: boryl anions of type NHC–B(CN)$^{2-}$, *Chem. Sci.*, 2017, **8**(9), 6274–6280.
58 P. Bissinger, H. Braunschweig, A. Damme, R. D. Dewhurst, K. Kraft, T. Kramer and K. Radacki, Base-Stabilized Boryl and Cationic Haloborylene Complexes of Iron, *Chem. – Eur. J.*, 2013, **19**(40), 13402–13407.
59 A. Doddi, M. Peters and M. Tamm, N-Heterocyclic, Carbene Adducts of Main Group Elements and Their Use as Ligands in Transition Metal Chemistry, *Chem. Rev.*, 2019, **119**(12), 6994–7112.
60 Z. Ye, C. Y. Kwok, S. L. Lam, L. Wu and H. Lyu, Copper-Catalyzed C–B(sp^3) Bond Formation through the Intermediacy of Cu–B(sp^3) Complex, *J. Am. Chem. Soc.*, 2025, **147**(18), 14915–14923.
61 C. Pranckevicius, C. Herok, F. Fantuzzi, B. Engels and H. Braunschweig, Bond-Strengthening Backdonation in Aminoborylene-Stabilized Aminoborylenes: At the Intersection of Borylenes and Diborenes, *Angew. Chem., Int. Ed.*, 2019, **58**(37), 12893–12897.
62 C. Pranckevicius, J. O. C. Jimenéz-Halla, M. Kirsch, I. Krummenacher and H. Braunschweig, Complexation and Release of N-Heterocyclic Carbene-Aminoborylene Ligands from Group VI and VIII Metals, *J. Am. Chem. Soc.*, 2018, **140**(33), 10524–10529.
63 J. T. Goettel and H. Braunschweig, Recent advances in boron-centered ligands and their transition metal complexes, *Coord. Chem. Rev.*, 2019, **380**, 184–200.
64 M. Brookhart, M. L. H. Green and G. Parkin, Agostic interactions in transition metal compounds, *Proc. Natl. Acad. Sci. U. S. A.*, 2007, **104**(17), 6908–6914.
65 P. Müller, P. Finkelstein, N. Trapp, A. Bismuto, G. Jeschke and B. Morandi, Nickel(I)–Phenolate Complexes: The Key to Well-Defined Ni(I) Species, *Inorg. Chem.*, 2023, **62**(41), 16661–16668.
66 R. C. Walroth, J. T. Lukens, S. N. MacMillan, K. D. Finkelstein and K. M. Lancaster, Spectroscopic Evidence for a 3d^{10} Ground State Electronic Configuration and Ligand Field Inversion in $[Cu(CF_3)_4]^{1-}$., *J. Am. Chem. Soc.*, 2016, **138**(6), 1922–1931.
67 R. Hoffmann, S. Alvarez, C. Mealli, A. Falceto, T. J. Cahill, T. Zeng III and G. Manca, From Widely Accepted Concepts in Coordination Chemistry to Inverted Ligand Fields, *Chem. Rev.*, 2016, **116**(14), 8173–8192.
68 G. Aullón and S. Alvarez, Oxidation states, atomic charges and orbital populations in transition metal complexes, *Theor. Chem. Acc.*, 2009, **123**(1), 67–73.
69 J. T. Boronski, A. E. Crumpton and S. Aldridge, A Crystalline NiX_6 Complex, *J. Am. Chem. Soc.*, 2024, **146**(51), 35208–35215.
70 E. Ramos-Cordoba, V. Postils and P. Salvador, Oxidation States from Wave Function Analysis, *J. Chem. Theory Comput.*, 2015, **11**(4), 1501–1508.
71 H. Braunschweig, M. A. Celik, R. D. Dewhurst, K. Ferkinghoff, A. Hermann, J. O. C. Jimenez-Halla, T. Kramer, K. Radacki, R. Shang, E. Siedler, F. Weißenberger and C. Werner, Interactions of Isonitriles with Metal–Boron Bonds: Insertions, Coupling, Ring Formation, and Liberation of Monovalent Boron, *Chem. – Eur. J.*, 2016, **22**(33), 11736–11744.
72 T. J. Hadlington, T. Szilvási and M. Driess, Striking transformations of the hydroborylene ligand in a HB:→NiII complex with isocyanides and CO, *Chem. Sci.*, 2018, **9**(9), 2595–2600.
73 C. Pranckevicius and D. W. Stephan, Ruthenium Complexes of an Abnormally Bound, Anionic N-Heterocyclic Carbene, *Chem. – Eur. J.*, 2014, **20**(22), 6597–6602.
74 G. Vijaykumar and S. K. Mandal, An abnormal N-heterocyclic carbene based nickel complex for catalytic reduction of nitroarenes, *Dalton Trans.*, 2016, **45**(17), 7421–7426.
75 G. Vijaykumar, A. Jose, P. K. Vardhanapu, S. P and S. K. Mandal, Abnormal-NHC-Supported Nickel Catalysts for Hydroheteroarylation of Vinylarenes, *Organometallics*, 2017, **36**(24), 4753–4758.
76 K. V. Tan, Z. Li, R. E. Karmis and P. J. Barnard, Selective Synthesis of Ni(II) and Pd(II) Complexes with either 'Normal' or 'Abnormal' N-Heterocyclic Carbene Coordination Modes, *ChemistrySelect*, 2018, **3**(10), 2830–2836.
77 I. A. Bhat, I. Avinash and G. Anantharaman, Nickel(II)- and Palladium(II)-NHC Complexes from Hydroxypyridine Functionalized C,O Chelate Type Ligands: Synthesis, Structure, and Catalytic Activity toward Kumada–Tamao–Corriu Reaction, *Organometallics*, 2019, **38**(8), 1699–1708.
78 (*a*) CCDC 2492761: Experimental Crystal Structure Determination, 2025, DOI: **10.5517/ccdc.csd.cc2pnxny**; (*b*) CCDC 2492762: Experimental Crystal Structure Determination, 2025, DOI: **10.5517/ccdc.csd.cc2pnxpz**; (*c*) CCDC 2492763: Experimental Crystal Structure Determination, 2025, DOI: **10.5517/ccdc.csd.cc2pnxq0**; (*d*) CCDC 2492764: Experimental Crystal Structure Determination, 2025, DOI: **10.5517/ccdc.csd.cc2pnxr1**; (*e*) CCDC 2492765: Experimental Crystal Structure Determination, 2025, DOI: **10.5517/ccdc.csd.cc2pnxs2**; (*f*) CCDC 2493820: Experimental Crystal Structure Determination, 2025, DOI: **10.5517/ccdc.csd.cc2pq0t8**.